


SHORT COMMUNICATION

Organ-specific immune response in lethal SARS-CoV-2 infection by deep spatial phenotyping

Akhila Balachander¹ , Bennett Lee¹, Subhra K Biswas¹, David C Lye^{2,3,4,5}, Raymond TP Lin², Yee-Sin Leo^{2,3,4,5,6}, Paul Chui⁷, Lisa FP Ng⁸ & Laurent Renia^{1,4,8,9}¹Singapore Immunology Network, Agency for Science, Technology and Research (A*STAR), Singapore City, Singapore²National Centre for Infectious Diseases, Singapore City, Singapore³Tan Tock Seng Hospital, Singapore City, Singapore⁴Lee Kong Chian School of Medicine, Nanyang Technological University, Singapore City, Singapore⁵Yong Loo Lin School of Medicine, Nanyang University of Singapore, Singapore City, Singapore⁶Saw Swee Hock School of Public Health, Singapore City, Singapore⁷Forensic Medicine Division, Health Sciences Authority, Singapore City, Singapore⁸A*STAR Infectious Diseases Labs, Agency for Science, Technology and Research (A*STAR), Singapore City, Singapore⁹School of Biological Sciences, Nanyang Technological University, Singapore City, Singapore**Correspondence**L Renia, A*STAR Infectious Diseases Labs,
A*STAR, 8A Biomedical Grove, Immunos
#03-11, Singapore City 138648, Singapore.
E-mail: renia_laurent@idlabs.a-star.edu.sgLFP Ng, A*STAR Infectious Diseases Labs,
A*STAR, 8A Biomedical Grove, Immunos
#04-06, Singapore City 138648, Singapore.
E-mail: lisa_ng@IDLabs.a-star.edu.sg

Received 31 July 2021;

Revised 30 January and 10 March 2022;

Accepted 11 March 2022

doi: 10.1002/cti2.1384

Clinical & Translational Immunology
2022; 11: e1384**Abstract**

Objectives. Immunopathology of ongoing COVID-19 global pandemic is not limited solely to pulmonary tissue, but is often associated with multi-organ complications, mechanisms of which are intensely being investigated. In this regard, the interplay between immune, stromal cells and cytokines in pulmonary and extrapulmonary infected tissues, especially in young adults (median age 46 years, range 30–53 years) without comorbidities, remains poorly characterised. **Methods.** We profiled lung, heart and intestinal autopsy samples from five SARS-CoV-2-infected cases for 18–20 targets to detect immune, cytokine and stromal cell status at subcellular resolution by a novel IHC-based deep-phenotyping technique, iSPOT (immunoSpatial histoPhenOmics using TSA-IHC), to assess spatial and functional patterns of immune response *in situ*, in lethal COVID-19 infection. **Results.** SARS-CoV-2-infected autopsy samples exhibit skewed counts of immune populations in all samples with organ-specific dysfunctions. Lung and ileal tissue reveal altered architecture with marked loss of tissue integrity, while lung and heart tissue show severe hyperinflammation marked by elevated TNF- α in heart tissue and additionally IL-6, IFN- γ and IL-10 cytokines in lung samples. **Conclusion.** With resurgence of infection in younger populations, single-cell cytokine localisation in immune and stromal structures provides important mechanistic insights into organ-specific immunopathology of naïve SARS-CoV-2 infection in the absence of other comorbidities.

Keywords: COVID-19, immunopathology, *in situ* spatial multiplexing, SARS-CoV-2 infection

INTRODUCTION

From the first detected case of COVID-19 infection caused by SARS-CoV-2 virus in China in December 2019, this pandemic has claimed > 6 million lives and continues to pose a global crisis.¹ While most infections are mild (81%) exhibiting flu-like symptoms, a reported 19% of patients experience severe to critical symptoms, the latter going into respiratory distress and multi-organ failure.² Vital to lethal pathogenicity is the ability of SARS-CoV-2 to suppress host antiviral immune responses³ such that infection elicits short, low-to-no antiviral interferons (IFNs),⁴ or detrimental delayed response.⁵ Dysregulated host response potentially leads to a build-up of viral burden at pulmonary sites of infection activating aberrant local immune responses, progressing to fulminant systemic cytokine storm eventually culminating in multi-organ failure and lethality.^{2,6}

A large number of studies have shed light on systemic immune responses to SARS-CoV-2 infection, specifically correlates of viral-induced hyperinflammation from analysis of peripheral blood as infection progresses from mild to lethality.^{7,8} Elevation in proinflammatory cytokines is a critical indication of severity and survival prognosis, especially that in TNF- α , IL-6 and IFN- γ .^{7,9} Peripheral responses are, however, distinct from compartment-specific responses assessed by bronchoalveolar lavage (BAL) extracts.^{10,11} While BAL samples serve as proxies of pulmonary reactions, they under-represent resident cells within the pulmonary parenchyma.¹² These site-specific responses underscore the importance of analysing disease correlates *in situ* to gain a more accurate understanding of pathology in tissues. To this end, we analysed autopsy samples from five young adult COVID-19 fatalities with no prior medical complications using a novel tyramide signal amplification (TSA)-IHC-based, deep multiplexing technique (iSPOT) to detect multiple targets including stromal cells, immune populations and inflammatory cytokines in pulmonary and extrapulmonary sites to characterise immunopathology *in situ*.

RESULTS

SARS-CoV-2-infected pulmonary tissues presented altered architecture with marked hypocellularity

All the patient and sample information is described in Table 1. A panel of 19 markers was used to

visualise tissue epithelium, endothelium and immune populations together with key cytokines, IL-6, TNF- α , IFN- γ and IL-10, implicated in severe COVID-19 infection (Figure 1a, Supplementary figure 1). PCA plots showed clear segregation of infected and uninfected phenotypes (Figure 1b). Histological examination of SARS-CoV-2 lungs revealed congested tissues with abundance of micro- and macrothrombi, diffuse alveolar damage, extensive hyaline membrane formation, and vascular and tissue damage in all infected cases (Figure 1c). Total tissue area was markedly increased because of membrane hyalinisation with distinct loss of reticulated lacunae seen in normal pulmonary tissues (Figure 1d, inset image). Virus-infected tissues displayed dramatic loss of cellularity (DAPI⁺ cells) across all cases (Figure 1d) including alveolar type 2 (AT2) epithelial (E-cadherin⁺), endothelial (CD31⁺) and immune (CD45⁺) compartments (Figure 1e). The density of CD14 marker expressed by immune, epithelial and endothelial cells was reduced in infected pulmonary tissues (Figure 1e). Within the immune compartment, virus-infected samples presented a substantial reduction in lymphoid T cells, especially CD8⁺ cytotoxic T cells (Figure 1f) and myeloid cells including macrophages (CD45⁺CD68⁺), dendritic cells (DC) (CD45⁺CD11c⁺CD68⁻) and notably neutrophils (CD45⁺CD11b⁺CD66b⁺) (Figure 1g). Taken together, SARS-CoV-2-infected pulmonary samples presented altered tissue architecture with marked loss of tissue integrity and hypocellularity characterised by a substantial reduction in stromal and immune cell numbers compared with normal uninfected lung tissue samples.

Detection of high levels of cytokines in SARS-CoV-2-infected pulmonary tissues

One of the important hallmarks of SARS-CoV-2 infection is elevation in levels of systemic proinflammatory cytokines. We therefore analysed *in situ* localisation and levels of IL-6, IFN- γ , TNF- α and IL-10 in the context of the viral spike protein and tissue stromal markers by iSPOT. All virus-infected samples were characterised by elevated levels of cytokines, with case-specific predominance. To gain a global perspective of cytokine levels, a thresholded histomask was built for each cytokine to compute the total fluorescence intensity associated with individual fields of view (Figure 2a, Supplementary figure 1). While Cases 1 and 2 exhibited high levels of IL-6,

Table 1. Patient clinical data and sample information

	Case 1	Case 2	Case 3	Case 4	Case 5
Age (years)	32	46	47	53	30
Gender	Male	Male	Male	Male	Male
Medical history/comorbidities	Nil	Nil	Nil	Nil	Nil
COVID-19 presentations during hospitalisation	Fever and difficulty breathing. Swabbed and sent home. Not hospitalised	Fever for 5 days with body ache, headache. Hospitalised on Day 1 of fever. On Day 5, fell from height from the hospital building	Chest tightness at residence. Went to bed and died in sleep. Not hospitalised	Stomach pain and vomited, followed by loss of consciousness. Failed resuscitation	Back pain and body ache. Fainted before being hospitalised. Failed resuscitation
Cause of death	Ischaemic heart disease	Multiple injuries because of fall	Ischaemic heart disease	Ruptured myocardial infarction	Coronary thrombosis
Autopsy review information (lung)	Early haemorrhagic diffuse alveolar damage with striking congestion of vessels. Extravasation of RBCs into alveoli. Hyaline membrane formation. Small haemorrhagic infarcts. Scanty inflammatory infiltrates (CD3 and CD4). Fibrin and platelet thrombi within small vessels. COVID-specific CD3 ⁺ and CD38 ⁺ detected near vessels	Early haemorrhagic diffuse alveolar damage; platelet and fibrin thrombi, focal lymphocytic vasculitis, mild emphysema (with interstitial thickening and focal aggregates of lymphocytes, which are CD3- and CD4-rich). Dilated vessels showed focal disruption of elastin	Heavy lungs 690 g/535 g. Markedly congested. Early haemorrhagic diffuse alveolar extravasation of RBCs. Predominant peribronchial lymphocytic infiltrates. Fibrin and platelet thrombi within smaller and intermediate vessels. Focal disruption of elastic lamina and dilatation present	Heavy lungs 839 g/560 g. Markedly congested. Sloughing of epithelium noted in the large airways. The pulmonary parenchyma shows severe congestion with areas of haemorrhage. Fibrin and platelet thrombi (MSB/CD61) within the smaller and intermediate vessels seen. Scanty and patchy inflammatory infiltrates noted	Severe congestion, with focal hyaline membrane formation. Occasional multinucleated giant cells present. Perivascular lymphocytic cuffing with dilatation of vessels and disruption of elastic lamina. Leaking capillaries with RBCs in alveolar spaces. Fibrin and platelet thrombi present in smaller vessels
Autopsy review information (heart)	Heart normal in size. Soft and flabby. Focal atherosclerosis in coronary vessel. Complete occlusion with the presence of fresh fibrin thrombi. Striking perivascular inflammatory infiltrate around small pericardial vessels, and into periaortal adipose tissue, involving tunica externa. Intramyocardial intravascular fibrin and platelet thrombi present. Patchy myocyte degeneration and fibrosis	Heart was normal in size. Coronary occlusion with pinpoint residual lumina. Initial and medial hypertrophy. No atherosclerotic plaques. Widespread myocyte necrosis with scattered lymphocytic infiltrates (CD3- and CD4-positive). Fibrin and platelet thrombi. Pericarditis present	Heart was moderately enlarged. Transmural pallor in anterolateral left ventricle wall. Left atrial occlusion. Severe occlusion of LCX. Mild atherosclerosis of RCA. Focal atherosclerosis of coronary with fresh fibrin thrombus. Moderately heavy mixed inflammatory infiltrate in perivascular adipose tissue infiltrating tunica externa and medial with clefting of wall. Patchy myocarditis, with mixed inflammatory infiltrate. Early granulation tissue present	Moderately enlarged heart. Mild atherosclerotic coronary disease. Coronary thrombosis in LAD. Transmural rupture in anterior–anteroseptal wall of LV. Coronary vessels show mediointimal hypertrophy associated with the presence of an occlusive thrombus. There is residual perivascular inflammation. The myocardium shows areas of haemorrhage with fibrin clots adherent to the endocardial surface. These are changes consistent with the observed myocardial rupture. The presence of areas where	Normal size heart. Coronary vessels showed recent mediointimal hypertrophy with occlusive fresh fibrin thrombus. Residual perivascular inflammation, with some vessels showing perivascular fibrosis. Myocardial vessels show intraluminal narrowing. Myocarditis present with mixed lymphocytic predominant infiltrate and myocyte necrosis. Patchy myocardial fibrosis present in mid-myocardium. Lymphocytic endocardial infiltrates and aggregates present

(Continued)

Table 1. Continued.

	Case 1	Case 2	Case 3	Case 4	Case 5
Autopsy review information (ileum)	Grossly normal with autolytic changes	Grossly normal with autolytic changes	Grossly normal with autolytic changes	Grossly normal with autolytic changes	Grossly normal with autolytic changes
	aggregates of intravascular fibrin and platelet thrombi (MSB and CD61) are seen. There are focal scanty perivascular lymphoid infiltrates. Small patchy fibrosis noted				

Control lung (US Biomax Inc., HuFPT131); Control heart (Novus Biologicals, NBP2-46893); Control ileum (OriGene CS803575)

Case 3 was dominated by elevated TNF- α and IFN- γ . We looked at cellular associations and sources of cytokines using Cases 1, 3 and 5 as examples (Figure 2b). Viral spike protein (VSP) was scarce in Cases 1 and 2 and highly abundant in Case 3. VSP was associated with macrophages and AT2 cells (Cases 1 and 3). All cases presented elevated levels of IFN- γ , and cells with intracellular IFN- γ co-expressed IL-10, possibly as a feedback mechanism to mitigate proinflammatory effects of IFN- γ (Cases 1, 3 and 5). IFN- γ was produced by CD3⁺ lymphocytes (all cases), but interestingly, the bulk of the cytokine signal was associated with CD11b⁺CD11c⁺ pulmonary macrophages and VSP⁺ AT2 epithelial cells (Cases 1 and 3). A closer examination revealed the presence of CD3 remnants in macrophages, indicating possible lymphocytic phagocytosis as a mechanism to control the production of IFN- γ . Case 3 presented high numbers of CD45⁺CD3⁻ IFN- γ ⁺ cells, which could possibly represent NK cells. TNF- α and IL-6 were associated primarily with endothelial and peri-endothelial cells (Case 3), with AT2 cells also producing TNF- α (Case 3). Macrophages potentially phagocytosing cellular debris or haemophagocytosis were also observed (Case 5). All examined pulmonary tissue samples presented hyperinflammation with the persistence of viral pathogen, indicating sustained immune responses to clear SARS-CoV-2 infection.

SARS-CoV-2-infected cardiac tissues are characterised by elevated proinflammatory cytokines

Cardiac complications are prevalent in SARS-CoV-2 infections; however, very few reports have characterised cardiac immunopathology and cytokine levels *in situ*. An 18-marker panel was used to multiplex cardiac autopsy samples (Figure 3a). Infected tissues did not present gross architectural changes compared with control tissues as shown by PCA plots (Figure 3b) and bright-field imaging (Figure 3c, Supplementary figure 1), nor were there any detectable differences in total tissue area and cellular densities (Figure 3d), although microthrombi were detected in Cases 1, 3 and 4 (Figure 3c). With the exception of Case 4 that presented extensive infiltration of CD4⁺ lymphocytes and CD11c⁺ dendritic cells, none of the other cases exhibited immune infiltration. A modest but consistent increase in numbers of vimentin⁺ fibroblasts and a decrease in numbers of cardiac

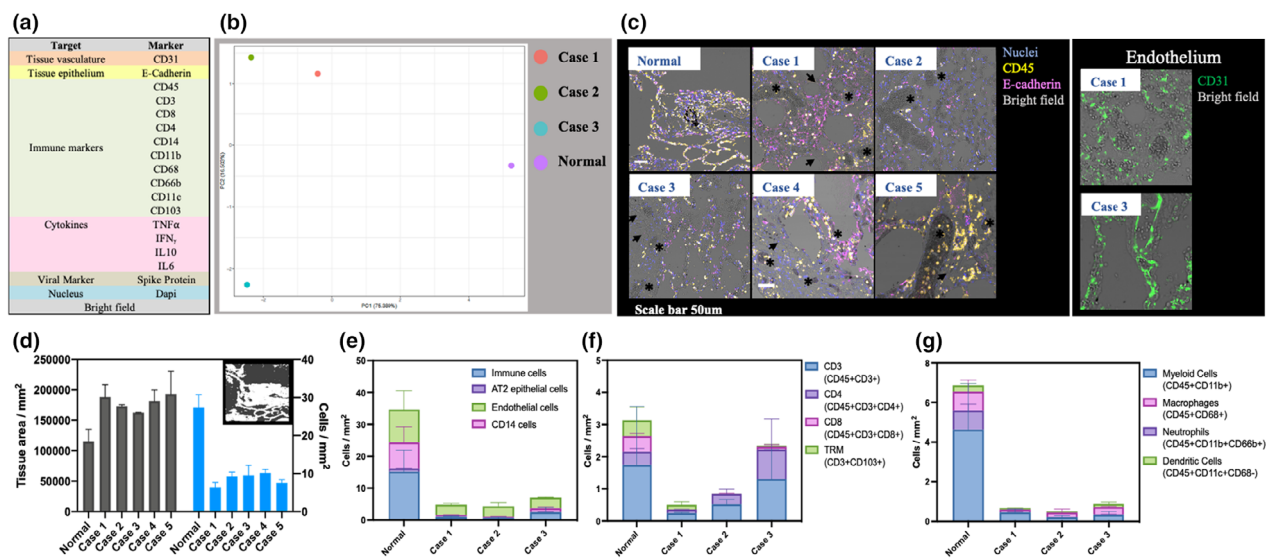


Figure 1. Immunopathology of SARS-CoV-2-infected pulmonary tissues. **(a)** Markers used in multiplexing panel. **(b)** PCA plot of normal and infected multiplexed pulmonary tissue samples. **(c)** Histological presentations in pulmonary tissue. The left panel is a composite of bright-field, CD45, E-cadherin and DAPI (nuclear) markers. * indicates clots, and → indicates hyaline membranes. Scale bar – 50 μm. The right panel is a composite of bright-field image and CD31 endothelial marker showing examples of fragmented endothelium with breaks. **(d)** Tissue area and cellular density normalised to acquired field of view and total tissue area, respectively. Insert is an example of histomask used to compute tissue area in field of view. **(e)** Density of stromal components. **(f)** Density of lymphoid T-cell populations. **(g)** Density of myeloid cell populations in normal and infected samples.

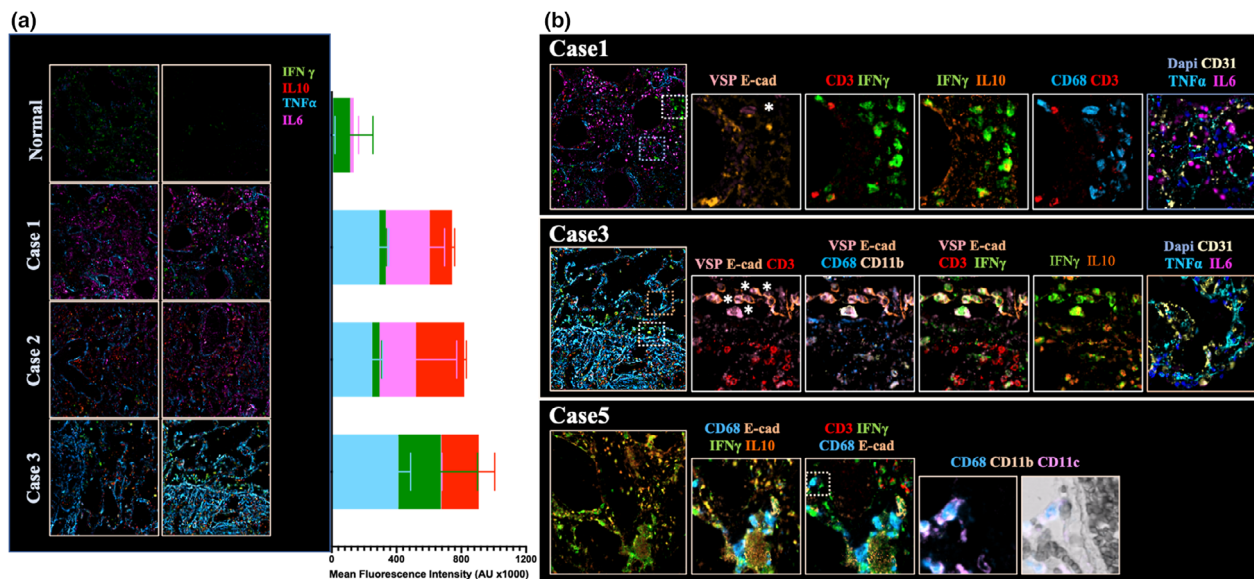


Figure 2. Cytokine profiles in SARS-CoV-2-infected pulmonary tissue. **(a)** Global cytokine profiles of acquired fields of view. **(b)** Case analysis of the localisation of cytokines and VSP (*) in SARS-CoV-2-infected cases. Regions of interest are colour-coded.

macrophages were observed across all SARS-CoV-2-infected samples (Figure 3e). VSP was detected in Cases 2 and 4; however, this was not associated with immune cells. The most striking and consistent feature of viral pathology in cardiac tissues was the

dramatic elevation in proinflammatory TNF-α levels accompanied by case-specific elevation in levels of IL-6, IFN-γ and IL-10 (Figure 3f). We describe Cases 2 and 4 as examples of cardiac pathology (Figure 3g). The bulk of the TNF-α signal was membrane-

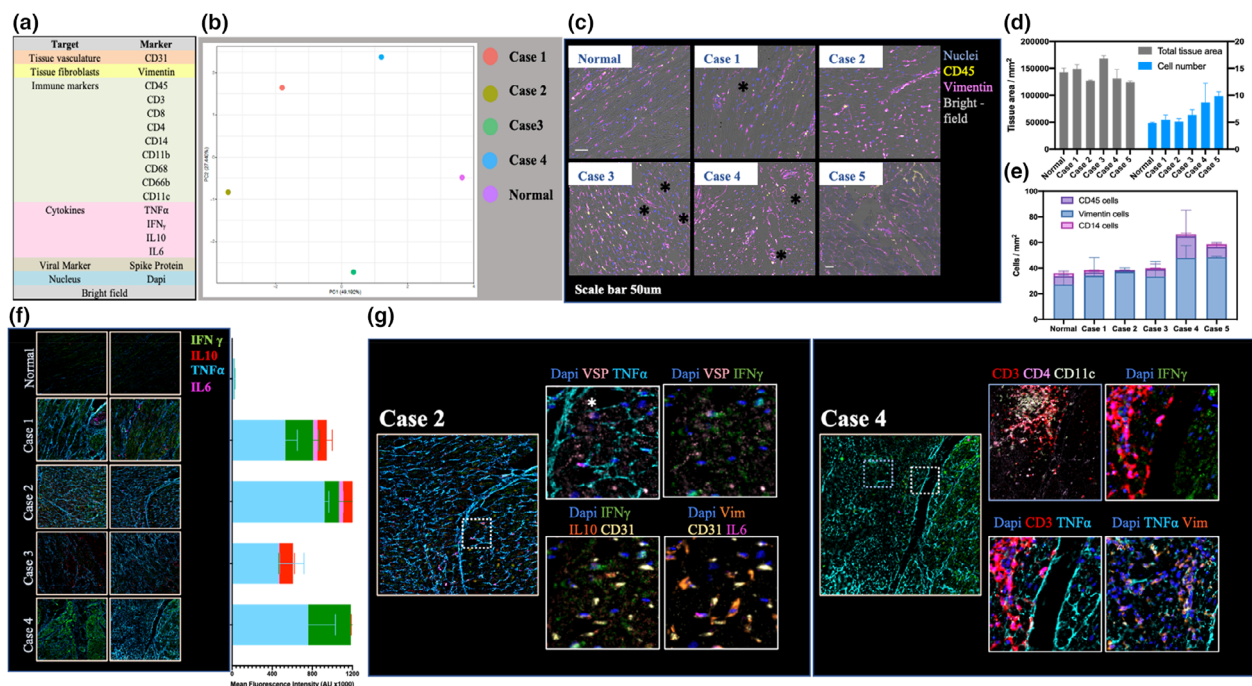


Figure 3. Cardiac immunopathology in SARS-CoV-2 infection. **(a)** Markers used in multiplexing panel. **(b)** PCA plot of normal and infected multiplexed cardiac tissues. **(c)** Histological presentations in cardiac tissue. Composite images of bright-field, CD45, vimentin and DAPI (nuclear) markers. * indicates thrombi. Scale bar – 50 μ m. **(d)** Tissue area and cellular density normalised to acquired field of view and total tissue area, respectively. **(e)** Density of stromal cell populations in normal and infected samples. **(f)** Global cytokine profiles of acquired fields of view. **(g)** Case analysis of localisation of cytokines and VSP (*) in SARS-CoV-2-infected cases.

associated, indicating the possibility of being brought in through systemic circulation (Cases 2 and 4). Intracellular TNF- α was detected in endothelial (CD31⁺) and fibroblasts (Vimentin⁺) cells (Case 2), which might serve as potential sources of the cytokine. IFN- γ signal was associated with large cells, perhaps cardiomyocytes (Case 2, 4) that were VSP⁺ (Case 2) in addition to CD3⁺ lymphocytes (Cases 2 and 4). The IL-10 signal was generally elevated in tissues, possibly also swept in through systemic circulation. IL-6 was detected in Cases 1, 2 and 5 with endothelial cells being the major source of the cytokine (Case 2). Although Case 4 presented marked infiltration of CD4⁺ lymphocytes, they were not IFN- γ -producing Th1 cells (Case 4). The infected cardiac samples presented distorted homeostatic counts of fibroblasts and macrophages with marked elevation in cytokine levels, especially TNF- α .

Enteric immunopathology in SARS-CoV-2 infection is associated with loss of germinal centres

Despite COVID-19 being a pulmonary infection, gastrointestinal symptoms are reported in some

patients.¹³ To better understand gastrointestinal manifestations, ileal autopsy samples were multiplexed using a marker panel (Figure 4a). Ileal tissues did not exhibit discernible histopathological presentations with no segregation of phenotypes in PCA plots (Figure 4b) or overt disorganisation in bright-field images (Supplementary figure 1). At the molecular level, the integrity of E-cadherin⁺ crypt structures was lost in all infected cases with thrombi detected in Cases 2 and 4 (Figure 4c). Most cases exhibited increased numbers of CD3⁺ and CD20⁺ lymphocytes (Figure 4d) without a consistent trend across infected cases. VSP was detected in Cases 1 and 5 of Peyer's patches probably taken up by M cells, with most cases presenting increased numbers of mononuclear phagocytes (MNP) (CD11c⁺ dendritic cells and CD68⁺ macrophages) (Figure 4e). No consistent trends in cytokine profiles were observed, although the levels were perturbed compared with uninfected control samples (Figure 4f). A significant observation consistent across all infected Peyer's patches was the poor formation of germinal centres (GCs) compared with control samples (Figure 4g), although all infected cases had comparable numbers of CD20 lymphoid cells.

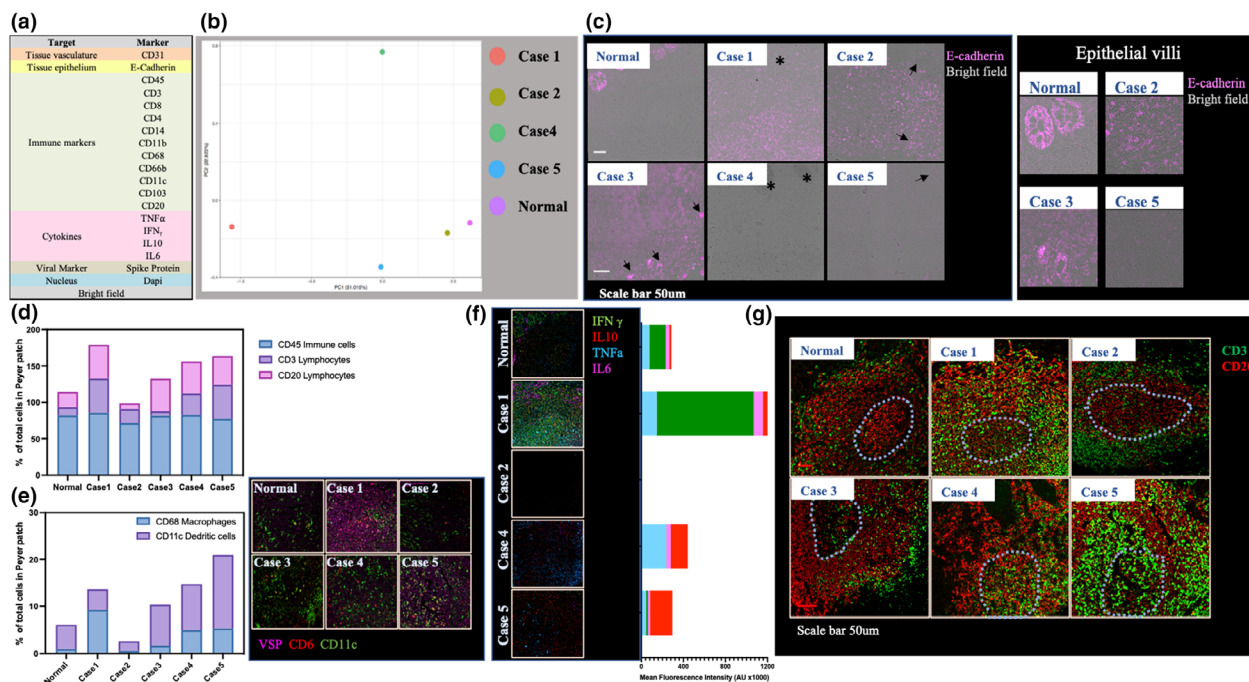


Figure 4. Enteric immunopathology in SARS-CoV-2 infection. **(a)** Markers used in multiplexing panel. **(b)** PCA plot of normal and infected multiplexed ileal tissues. **(c)** Histological presentations in ileal tissue. Composite images of bright-field and E-cadherin markers. * indicates clots, and \rightarrow indicates epithelial villi. Scale bar – 50 μ m. The right panel is a zoomed image of E-cadherin crypts. **(d)** Immune cell numbers in intrafollicular Peyer’s patches. **(e)** VSP and mononuclear phagocyte localisation and numbers in Peyer’s patches. **(f)** Global cytokine profiles of acquired fields of view. **(g)** Germinal centres indicated in blue-dotted contour in normal and infected samples.

DISCUSSION

Our deep quantitative *in situ* characterisation of SARS-CoV-2-infected pulmonary and extrapulmonary tissues provides important insights into immunopathology and dysregulation in lethal disease. This study is particularly relevant as cases examined are young adults aged 30–53 years with no prior medical conditions. Most histopathological analyses of SARS-CoV-2 cases in the literature are from aged cohorts (> 65 years) with comorbidities where single-to-few immune cell types have been profiled to describe clinical presentations.^{14,15} Rendeiro *et al.*¹⁶ recently published an extensive *in situ* characterisation of SARS-CoV-2 pulmonary infection by imaging mass cytometry in an old age cohort (mean age of 62 years) with a partial overlapping panel of markers. We observe similar changes in tissue architecture with marked elevation in tissue cytokines indicating that, in lethal infection, SARS-CoV-2 pathology has a dominant effect on both age-related frailty and comorbid conditions. Systemic elevation in levels of proinflammatory cytokines is important for viral clearance, as seen in patients with mild-to-severe

infection⁷; however, failure to clear pulmonary SARS-CoV-2 viral burden leads to persistence and aggravated fuelling of hypercytokinaemia that can exert synergistic maladaptive effects leading to lethality. Additionally, the production of TNF- α and IL-6 by peri-endothelial and endothelial cells in pulmonary and cardiac samples observed in this study is indicative of severely dysregulated vascular tone capable of eliciting coagulopathies.¹⁷

Cardiac abnormalities are prevalent in COVID-19 infections with up to 55% of cases presenting cardiac disorders including patients who have no prior cardiac history.¹⁸ Four of five cases in our cohort succumbed because of cardiac dysfunction. The histopathological analysis of SARS-CoV-2 cardiac tissues so far has described occasional mononuclear infiltrates^{19,20}; however, our study shows a more systematic regression in numbers of macrophages, essential homeostatic regulators of cardiac health²¹ with increased numbers of vimentin⁺ cells potentially indicative of myofibroblast differentiation during cardiac injury.²² A key and consistent feature of infected cardiac samples is elevation in TNF- α levels. TNF- α and IL-6 are covariant factors in cardiac pathology, and TNF- α is a prognostic indicator of

failing heart.²³ Serum from COVID-19 patients has been shown to induce diastolic dysfunction predominantly mediated by IFN- γ in human cardiac organoids.²⁴ A cocktail of proinflammatory factors together with skewed counts of homeostatic cells can evidently result in detrimental cardiac health and lethal dysfunctions in SARS-CoV-2 infection.

Gastrointestinal symptoms are experienced by ~12% of SARS-CoV-2-infected patients, presenting loss of appetite, diarrhoea and nausea¹³; however, no gross histological abnormalities have been reported, especially with regard to Peyer's patches that are sentinels of enteric infections in the gut. Germinal centres (GCs) within Peyer's patches are important for eliminating gut-associated pathogens and maintaining tolerance to commensal microflora.²⁵ Degeneration of lymphoid tissues such as thoracic lymph nodes and spleen has been shown to compromise humoral immunity in early COVID-19 infection.²⁶ From our study, disrupted GCs of Peyer's patch could also contribute to dysregulated gut immune response in COVID-19 infection.

From a system point of view, a recent report identified the synergistic effect of TNF- α and IFN- γ as being necessary and sufficient in mediating cell death and multi-organ damage akin to COVID-19 presentations through PANoptosis engaging apoptotic, pyroptotic and necroptotic pathways in murine models.²⁷ We show in our study a snapshot of multi-organ and multifactorial complexities in SARS-CoV-2 infection using iSPOT, a novel, highly sensitive IHC method that enables detection, localisation and quantification of large numbers of targets by fluorescence imaging across tissue types. Given the interplay of several proinflammatory cytokines in pathology of SARS-CoV-2 infection, combinatorial cytokine therapies may be an option that could benefit young patients, especially with progressive severity.

METHODS

Patient clinical data and sample information

Autopsy samples of lung, ileum and heart from five COVID-19 fatalities were collected and processed as part of coronial death investigations at the Forensic Medicine Division, Health Sciences Authority, as per regulatory guidelines. Viral infection was confirmed by PRC testing. Paraffin blocks from organs were prepared. Four- to five- μ m-thick FFPE sections from 8 to 10 blocks of lung samples, a minimum of four and two blocks each from the heart and ileal samples, respectively, were examined for each case.

One representative section per organ per patient was analysed by iSPOT multiplexing. All cases in this study were men aged between 30 and 53 years with no prior medical conditions.

Normal adult tissue samples, one each for lung (US Biomax Inc., HuFPT131), heart (Novus Biologicals, NBP2-46893) and ileum (OriGene CS803575), were used as reference controls. All patient clinical data and sample information are described in Table 1.

iSPOT multiplexing

FFPE sections were deparaffinised by baking at 60°C for 30 min. The slides were treated with HistoChoice Clearing Agent (VWR Life Science, Avantor) for 5 min twice and 100% ethanol for 3 min thrice, followed by serial rehydration in 95%, 70% and 50% ethanol for 3 min each. Samples were fixed in 10% NBF (Richard-Allan Scientific, Thermo Scientific) for 10 min, washed in water and retrieved. iSPOT multiplexing was performed by iteratively probing for targets by TSA-IHC detection and image acquisition followed by chemical inactivation of fluorophores as described in the patent (Patent Application No. 10202106710X). Antibodies used are listed in Supplementary table 1. Tissue sections were imaged using Olympus IX83 slide scanner with 20 \times objective (NA0.8) as 500- μ m² tiled images. Two such regions of interest were imaged for every tissue sample. Of the 18 tissue samples (5 infected and 1 normal tissue per organ), Cases 4 and 5 of lung, Case 3 of ileum and Case 5 of heart were used to initially optimise experimental conditions, validate antibody staining and test feasibility. These samples were probed for a smaller panel (Supplementary table 2) and imaged using Olympus Confocal FV1000 System at 20 \times (NA0.7), zoom 2. For pulmonary tissue optimisation, 2 \times 250 μ m² images were acquired for each case. In the pilot experiments, we did not detect any signal for Foxp3 and granzyme B in any of the tested tissues indicating a lack of Treg cells and activated CD8⁺ cytotoxic T cells and/or natural killer (NK) cells. Hence, FOXP3 and granzyme B were omitted from the final multiplexing panel.

Image processing, segmentation, gating and quantification

All the images were background-subtracted using a rolling ball radius of 20 pixels, registered and transformed using the ImageJ software to compile composite images (Supplementary figure 1). The composite images were imported into StrataQuest (SQ, V6, TissueGnostics, Vienna, Austria), segmented and gated to perform gating analysis. Nuclear segmentation was used to identify and segment all the cellular markers. For all samples, epithelial (E-cadherin⁺) or fibroblast (Vimentin⁺), endothelial (CD31⁺) and immune cells (CD45⁺) were gated from the nuclear segmented objects. All the immune populations were quantitated using the CD45 gate. For ileal samples, all the populations were gated on nuclei. Gate settings from control samples were propagated across respective SARS-CoV-2-infected tissue samples to quantitate cell populations for each tissue type. Data from cases used in optimisation run have been used for limited interpretations where applicable only.

Histomask

A mask was constructed over each of the bright-field images to compute the total tissue area in each field of view using the SQ software. This was performed by thresholding on each of the bright-field images, followed by 'morphological masking' and 'dilate and close areas' functions with a diameter of 10 μm . The total tissue area of the mask was computed and normalised per mm^2 taking into consideration the dimension of field of view.

Principal component analysis

Intensity values associated with segmented nuclei were logarithmically transformed to assume normal distribution and averaged from multiple ROIs for each sample prior to principal component analysis (PCA) using the `prcomp` function in R version 3.6.2. As intensity values between images acquired at the slide scanner were ~ 10 -fold higher than for images from the confocal system, only cases acquired at the slide scanner were used for PCA.

ACKNOWLEDGMENTS

This study was funded by the core grants from Singapore Immunology Network (SigN), A-STAR Infectious Diseases Labs (ID Labs), Agency for Science, Technology and Research (A*STAR), and NMRC grant no. COVID19RF-001. We thank group members of Professor Laurent Renia and Dr Lisa FP Ng for their help with reagent procurement and sample collection, respectively.

CONFLICT OF INTEREST

The authors declare no conflict of interest.

AUTHOR CONTRIBUTIONS

Akhila Balachander: Conceptualization; Formal analysis; Investigation; Methodology; Writing – original draft. **Bernett Lee:** Formal analysis; Writing – review & editing. **Subhra K Biswas:** Funding acquisition; Supervision; Writing – review & editing. **David C Lye:** Writing – review & editing. **Lisa FP Ng:** Funding acquisition; Project administration; Resources; Supervision; Writing – review & editing. **Laurent Renia:** Conceptualization; Funding acquisition; Project administration; Writing – review & editing.

REFERENCES

- Dong E, Du H, Gardner L. An interactive web-based dashboard to track COVID-19 in real time. *Lancet Infect Dis* 2020; **20**: 533–534.
- Gupta A, Madhavan MV, Sehgal K *et al.* Extrapulmonary manifestations of COVID-19. *Nat Med* 2020; **26**: 1017–1032.
- Banerjee AK, Blanco MR, Bruce EA *et al.* SARS-CoV-2 disrupts splicing, translation, and protein trafficking to suppress host defenses. *Cell* 2020; **183**: 1325–1339 e21.
- Blanco-Melo D, Nilsson-Payant BE, Liu W-C *et al.* Imbalanced host response to SARS-CoV-2 drives development of COVID-19. *Cell* 2020; **181**: 1036–1045 e1039.
- Lee JS, Park S, Jeong HW *et al.* Immunophenotyping of COVID-19 and influenza highlights the role of type I interferons in development of severe COVID-19. *Sci Immunol* 2020; **5**: eabd1554.
- Tay MZ, Poh CM, Renia L, MacAry PA, Ng LFP. The trinity of COVID-19: immunity, inflammation and intervention. *Nat Rev Immunol* 2020; **20**: 363–374.
- Liu J, Li S, Liu J *et al.* Longitudinal characteristics of lymphocyte responses and cytokine profiles in the peripheral blood of SARS-CoV-2 infected patients. *EBioMedicine* 2020; **55**: 102763.
- Chen G, Wu DL, Guo W *et al.* Clinical and immunological features of severe and moderate coronavirus disease 2019. *J Clin Invest* 2020; **130**: 2620–2629.
- Del Valle DM, Kim-Schulze S, Huang H-H *et al.* An inflammatory cytokine signature predicts COVID-19 severity and survival. *Nat Med* 2020; **26**: 1636–1643.
- Bost P, De Sanctis F, Canè S *et al.* Deciphering the state of immune silence in fatal COVID-19 patients. *Nat Commun* 2021; **12**: 1428.
- Xu G, Qi F, Li H *et al.* The differential immune responses to COVID-19 in peripheral and lung revealed by single-cell RNA sequencing. *Cell Discov* 2020; **6**: 73.
- Yu Y-R, Hotten DF, Malakhau Y *et al.* Flow cytometric analysis of myeloid cells in human blood, bronchoalveolar lavage, and lung tissues. *Am J Respir Cell Mol Biol* 2016; **54**: 13–24.
- Zhong P, Xu J, Yang D *et al.* COVID-19-associated gastrointestinal and liver injury: clinical features and potential mechanisms. *Signal Transduct Target Ther* 2020; **5**: 256.
- Borcuk AC, Salvatore SP, Seshan SV *et al.* COVID-19 pulmonary pathology: a multi-institutional autopsy cohort from Italy and New York City. *Mod Pathol* 2020; **33**: 2156–2168.
- Bryce C, Grimes Z, Pujadas E *et al.* Pathophysiology of SARS-CoV-2: targeting of endothelial cells renders a complex disease with thrombotic microangiopathy and aberrant immune response. *medRxiv* 2020. <https://doi.org/10.1101/2020.05.18.20099960>
- Rendeiro AF, Ravichandran H, Bram Y *et al.* The spatial landscape of lung pathology during COVID-19 progression. *Nature* 2021; **593**: 564–569.
- Iba T, Levy JH, Connors JM, Warkentin TE, Thachil J, Levi M. The unique characteristics of COVID-19 coagulopathy. *Crit Care* 2020; **24**: 360.
- Dweck MR, Bularga A, Hahn RT *et al.* Global evaluation of echocardiography in patients with COVID-19. *Eur Heart J Cardiovasc Imaging* 2020; **21**: 949–958.
- Bryce C, Grimes Z, Pujadas E *et al.* Pathophysiology of SARS-CoV-2: the Mount Sinai COVID-19 autopsy experience. *Mod Pathol* 2021; **34**: 1456–1467.
- Lindner D, Fitzek A, Bräuninger H *et al.* Association of cardiac infection with SARS-CoV-2 in confirmed COVID-19 autopsy cases. *JAMA Cardiol* 2020; **5**: 1281–1285.
- Swirski FK, Nahrendorf M. Cardioimmunology: the immune system in cardiac homeostasis and disease. *Nat Rev Immunol* 2018; **18**: 733–744.
- Zeisberg EM, Kalluri R. Origins of cardiac fibroblasts. *Circ Res* 2010; **107**: 1304–1312.

23. Torre-Amione G, Kapadia S, Benedict C, Oral H, Young JB, Mann DL. Proinflammatory cytokine levels in patients with depressed left ventricular ejection fraction: a report from the studies of left ventricular dysfunction (SOLVD). *J Am Coll Cardiol* 1996; **27**: 1201–1206.
24. Mills RJ, Humphrey SJ, Fortuna PRJ *et al.* BET inhibition blocks inflammation-induced cardiac dysfunction and SARS-CoV-2 infection. *Cell* 2021; **184**: 2167–2182 e2122.
25. Mowat AM. Anatomical basis of tolerance and immunity to intestinal antigens. *Nat Rev Immunol* 2003; **3**: 331–341.
26. Kaneko N, Kuo HH, Boucau J *et al.* Loss of Bcl-6-expressing T follicular helper cells and germinal centers in COVID-19. *Cell* 2020; **183**: 143–157 e113.
27. Karki R, Sharma BR, Tuladhar S *et al.* Synergism of TNF- α and IFN- γ triggers inflammatory cell death, tissue

damage, and mortality in SARS-CoV-2 infection and cytokine shock syndromes. *Cell* 2021; **184**: 149–168.

Supporting Information

Additional supporting information may be found online in the Supporting Information section at the end of the article.



This is an open access article under the terms of the Creative Commons Attribution-NonCommercial License, which permits use, distribution and reproduction in any medium, provided the original work is properly cited and is not used for commercial purposes.